RESEARCH ARTICLE - HYDROLOGY

# Laboratory study of the effects of terrestrial coastal forests on the absorption of solitary wave force

Golnaz Mirzakhani[1] · Elham Ghanbari-Adivi[1] · Rohollah Fattahi[1]

## Abstract

One of the beach protection techniques is using natural methods based on the coastal ecosystem. Studies show the reducing effect of forest covers on wave destruction intensity in different areas. However, it is not yet well understood how various densities of terrestrial coastal forest (TCF) affect the wave attenuation and reduce their strength. Studying the impact of various forest parameters, such as density, distance, and arrangement type on the wave force attenuation, this research measures the wave forces directly. TCF model was installed in a knife edge flume, which equipped with a load cell and an acoustic Doppler velocimeter. The experiments were performed in two staggered and parallel arrangements consisting of different densities from 12 to 273 stems per unit area. Based on obtained results, TCF had significant effects on the wave force absorption. An increase in the number of trees (density) increased TCF resistance force and the absorbed wave force. In its best, the TCF could absorb the wave force 3.76 times more than the no-TCF case. It could reduce the wave height by up to 81% at the highest density and maximum wave height. The absorbed wave force and drag coefficient rose as the number of rows of trees opposing the flow decreased and the intervals between trees were shortened. Increasing tree density from 12 to 273 stems per unit area increased the drag coefficient by the average of 61.82% for parallel and staggered arrangements, which means an average increase of 9.7% for each TCF row.

**Keywords** Coastal defense · Drag coefficient · Force · Nature-based solution · Terrestrial forest · Wave

## Introduction

Coastal areas form dynamic ecosystems at the land–sea interface (Leewis et al. 2012; Gonçalves et al. 2013; Martins et al. 2013). An important feature of these areas is their variability (Dias 2004) in terms of the exposure to many natural and human-made pressures (Nobre and Ferreira 2009). Among several non-structural and structural coast protection methods, the latter have detrimental effects on coastal environment (Fathi-Moghadam et al. 2018).

Slopes far from the ocean, and places behind the dunes are the coastward sheltered areas were coastal forests form. Although the latter do not undergo daily salt spraying, they

are affected by storm winds and salts (Temmerman et al. 2013). Coastal forest is commonly used as an effective approach against natural and human-made disturbances (Gaertner-Mazouni and De Wit 2012; Nanko et al. 2019), the capacity of which was not studied in all aspects (Turker et al. 2006). To date, the best known effect of forest in coastal areas is the attenuation of sea waves (Mendez and Losada 2004). Coastal trees as palm (Vanderpuye and Armah 1997), coconut (Rajendra and Sumariati 2018), and pine (Torita et al. 2022; Jalil-Masir et al. 2022) can protect the coast against waves. Vegetation not only reduces wave destructive effects (Leonardi et al. 2018; Möller et al. 2014; Temmerman et al. 2013; Morris et al. 2018) and storm effects (Wamsley et al. 2009) on natural coasts and coastal defense structures (Winterwerp et al. 2020; Mu et al. 2019), but also strengthens the natural habitats (Nordstrom 2014) and provides recreational opportunities (Foster et al. 2013).

Wave-forest interactions were simulated under laboratory-controlled conditions with natural (Tschirky et al. 2001) or artificial vegetation (Huang et al. 2011; Cavallaro et al. 2011; Augustin et al. 2009). Zinke et al. (2011) believed

✉ Elham Ghanbari-Adivi
ghanbariadivi@sku.ac.ir

1 Department of Water Science Engineering, Shahrekord University, Shahrekord, Iran

that correct parameterization of flow resistance by vegetation was the most important uncertainty factor. Modeling a tree with a flexible structure (Fathi Moghadam et al. 2018) or with a rigid structure (Akgul et al. 2013; Sundar et al. 2011) is a reason why the real and model specimens differ.

According to studies, palm and coconut trees are effective in reducing the harmful effects of waves in coastal regions (Mascarenhas and Jayakumar 2008). The flexibility parameter is expected to have little influence on wave characteristics owing to the tree structure and, therefore, the flow structure; hence, rigid cylinders are often employed to describe these trees. Thus, the effects of coastal forest on damping of waves were evaluated via the extensive field or wave-flume laboratory studies, and the integrated coast-forest-wave simulation.

To quantify these effects, several field studies were performed in various areas, including salt marshes in the USA (Knutson et al. 1982); tidal areas in the UK (Möller et al. 1999; Möller and Spencer 2002); mangrove coastal forests in Vietnam (Mazda et al. 2006; Quartel et al. 2007; Nguyen and Parnell 2017); shallow lakes in Sweden (Lovsted and Larson 2010); southern coasts of the Pacific Ocean in Indonesia and New Guinea (Hirashi and Harada, 2003; Grilli et al. 2020); and northern coasts of the Arctic Ocean in Norway and Russia (Sinitsyn et al. 2020). Similar results were yielded to reduce the wave height significantly in the areas with forest cover compared with those without forest cover.

Several experimental studies were conducted on the vegetation-caused wave attenuation. Esteban et al. (2020) studied the bed roughness effect on the coastal wave propagation and water level rise; they suggested that such experiments be performed on uneven beds with a Manning coefficient of about 0.06. When waves hit the coast, the turbulence intensity changes (Lou et al. 2018) and the wave velocity falls (Hu et al. 2014). Turbulence plays an important role to describe the physical process of cover-through flow (Zhang et al. 2013; Wang et al. 2015). Chen et al. (2020) studied the changes in wave velocity and turbulence by rigid vegetation and proposed a formula to predict the stem-scale turbulence using velocity, drag coefficient, and vegetation density and diameter. Möller et al. (2014) assessed the energy loss in a reservoir with natural lagoon vegetation under long-wave conditions in the laboratory and came to the conclusion that up to 60% of the observed wave height decrease might be attributable to the vegetation. Yin et al. (2017) found, by experimental studies on coast vegetation, that damping coefficient increased with an increase in the number of rows and in the relative density.

The dependence of wave damping rate on the forest density indicates the forest performance at a certain area, which can be examined by the drag coefficient as a representative of the resistance against the flow (Hirashi and Harada 2003). In fact, the wave energy loss is mainly related to the forest-caused drag force (FD) that can be defined quantitatively

by the Morison equation (Dalrymple et al. 1984; Morison et al. 1950). In the vegetation-wave interaction simulation, choosing the appropriate value for the forest drag coefficient (Cd), which has a significant impact on the FD, is crucial for an accurate wave damping prediction (Cao et al. 2015; Maza et al. 2015). This study aims to obtain a relationship capable of predicting the group drag coefficient in terms of tree cover under known wave height conditions. The effect of different characteristics of waves and vegetation was addressed in several studies.. Despite any vegetation diversity, the changes in the wave damping by the coastal forest are significant (Mendez and Losada 2004). Lima et al. (2007) obtained increased wave damping values for forests with higher densities. Porosity effect of vegetation compaction causes waves to reflect and reduce their heights. Although the inertial force leads to the energy loss and reduction of damping capacity of the vegetation, overall, the wave damping is still rising (Suzuki et al. 2019). The damping effect of the wave height was not clearly explained; initial results of a study by Cavallaro et al. (2011) showed that an increase in the inflow wave height increased the wave damping while the observations by Bradley and Houser (2009) estimated less damping increase at more inflow wave heights. This issue is examined. Van veelen et al. (2020) studied the effect of forest flexibility and showed that wave weakening effect of flexible cover is 20–70% less than that of rigid cover due to wave's passing through the flexible cover. Flexible cover has no impact on the velocity profile, but stiff cover changes it. According to Wang et al. (2019), leaves are more effective than stems in reducing wave transmission and height changes. In actuality, a flexible surface's element's flow energy is lower than a rigid surface's (Toloui et al. 2019). Based on the literature review, most related studies have focused on submerged vegetation or salt marsh and swamp plants rather than on terrestrial coastal forest (TCF) to examine mentioned parameters. This research attempts to fill the gap by emphasizing the role of TCF in significant reduction of destructive effects of coastal waves. However, more empirical and numerical studies are needed to provide the design criteria for coastal vegetation development.

The idea of a flume with knife edge supports and capability of performing freely in any flume under motion threshold conditions so that the contact friction could be kept at a zero level, is first defined and used. The wave force absorbed by the coastal forest is directly measured.

This research attempts to fill the gap by emphasizing the role of TCF in significant reduction of destructive effects of coastal waves. In particular, this study aims to simulate the TCF, measure the force absorbed from long waves by terrestrial coastal forest, and determine the total drag coefficient and wave damping rate based on breaking solitary waves, which denotes waves breaking on the coast before reaching the TCF.

## Materials and methods

### Dimensional analysis

The parameters that influenced the hydraulics of the phenomenon were included: coast slope ($S$); coast still water level ($d_0$); fluid density ($\rho$); fluid viscosity ($\mu$); gravity acceleration ($g$); tree diameter ($D$); the width of the TCF parallel to the wave direction ($BG$); TCF length along the flume width ($L$); TCF density number ($D_v$); tree height ($hv$); absorbed wave force in the presence of the TCF ($F$), which is assumed to equal the drag force (FD); absorbed wave force in the absence of the TCF ($F_0$); shear stress by the cover ($\tau_v$); wave propagation velocity ($V$); wave height ($H$); and damped wave height ($H_0$):

Parameters effective in such issues as the drag coefficient and cover resistance against flow can be related in the form of Eq. (1).

$$f_1\left(S, d_0, \rho_w, \mu_w, g, D, BG, L, D_v, \tau_v, h_v, F_0, F, V, H, H_0\right) = 0 \tag{1}$$

Next, the Buckingham π method (Buckingham 1914) was used to extract dimensionless parameters from Eq. (2):

$$f_2\left(\frac{F}{\rho_w H^2 V^2}, \frac{\rho_w HV}{\mu_w}, \frac{\tau_v}{\rho_w V^2}, \frac{V}{\sqrt{Hg}}, \frac{BG}{L},\right.$$
$$\left.\frac{H}{h_v}, \frac{H}{D}, \frac{F - F_0}{F_0}, \frac{H}{H_0}, D_v, S\right) = 0. \tag{2}$$

The obtained dimensionless parameters were then examined to omit $Fr$ (Froude Number) and $Re$ (Reynolds Number), flow nature and flow turbulence, respectively.

Omitting constant parameters, dimensionless numbers with little effect, and those overlapping with other numbers during the experiment resulted in Eq. (3):

$$C_d = f_3\left(\frac{\tau_v}{\rho_w V^2}, \frac{H}{h_v}\right). \tag{3}$$

Based on the studies by Nardin et al. (2016) and Baptist (2005) on investigating the forest cover effects on the flow, Eq. (3) is used to estimate $\tau_v$ presented in Eq. (4):

$$\tau_v = \frac{1}{2}\rho C_d D D_s h_v V^2, \tag{4}$$

where $\tau_v$ is the shear stress by the cover, $C_d$ is the drag coefficient, $D$ is the tree diameter, $D_s$ is the stem density (number of stems per unit area), $h_v$ is the cover height, and $V$ is the flow velocity in the forest.

Then, dimensionless parameters $F_t$ and $K_v$ (Eqs. 5 and 6), obtained through dimensional analyses, were used to study the effects of the TCF on reducing wave force and wave

height, respectively. In fact, $F_t$ indicates TCF performance and $K_v$ is used as wave dissipation rate.

$$F_t = \frac{F - F_0}{F_0} \tag{5}$$

$$K_v = \frac{H}{H_0} \tag{6}$$

### Drag force theory

The inflow wave gradually turns into an unstable current that expands above the shallow water near the coastline (Fathi-Moghadam et al. 2018). Upon hitting the TCF, this inflow wave exerts two forces on the trees: (1) drag force that is equal to wave absorbed force (the first term in Eq. 7) due to the wave velocity and (2) inertial force (the second term in Eq. 7) due to the flow acceleration; Eq. (7) can be used to estimate the total hydrodynamic force ($F_{\text{TL}}$) (Morison et al. 1950):

$$F_{\text{TL}} = 0.5\rho C_d A_p |V|V + \rho C_m \forall\left(\partial V / \partial t\right), \tag{7}$$

where $\rho$ is the fluid density, $C_d$ is the drag coefficient, $A_P$ is the flow-front tree area, $V$ is the wave-induced particle velocity (equal to wave velocity before breaking), $C_m$ is the inertia coefficient, $\forall$ is the flow-front tree volume, and $(\frac{\partial V}{\partial t})$ is the time-based velocity variations.

The total instantaneous hydrodynamic force exerted on the tree throughout the streamline includes the drag force and the inertia force. Sorensen (2006) believed that since the temporal inertia ($\frac{\partial V}{\partial t}$) is negligible in the shallow water, so is the inertial force equation because it is a function of ($\frac{\partial V}{\partial t}$). This was confirmed by a laboratory study by Hirashi and Harada (2003), in which the pressure difference between the two sides of the vegetation was explained to be mainly due to the drag resistance. This study too neglected the very small $\left(\frac{\partial V}{\partial t}\right)$ assuming quasi-steady flow (Husrin et al. 2012) and simplified Eqs. (7) to (8). In other words, the total instantaneous hydrodynamic force exerted on the tree through the streamline can be the drag force (Fathi-Moghadam et al. 2018).

$$F_{TL} = F = 0.5\rho C_d A_P V^2 \tag{8}$$

Using Eq. (9), the drag coefficient can be calculated as follows:

$$C_d = \frac{2F}{\rho A_p V^2}. \tag{9}$$

## Experimental detail

### Tools and equipment

Experiments were performed in a laboratory flume of 8.6 m long, 0.6 m wide, and 0.6 m height composed of a metal floor and Plexiglas walls. Water from the main water pipe was pumped via a connecting pipe into the wave tank in the flume.

The solitary wave theory was used to produce the waves that were the subject of this study. In recent decades, single-wave modeling of tsunami wave impacts and their propagation to coastal regions have drawn a lot of interest (Hsiao and Lin 2010). An important reason for this simulation is the transmission property of solitary waves (Chang and Hwung 2006). Here, two sliding gates were installed in a 2-m distance of the flume to create a reservoir where water could be regulated at different levels and waves with known heights could be created by quick gate opening. This method was first proposed by Russell (1845) and later applied in other studies by Ratnosooriya et al. (2008) and Jalil-Masir et al. (2021).

To measure the force used to the coast, a moving plate was equipped with a 50-kg-capacity dynamic load cell of class C3 measurement accuracy with 0.023% error installed in front of the knife edge flume to transfer the instantaneous wave force exerted to the moveable plate and TCF model to the PM-LD01 electronic display.

To measure the velocity, received information and signals were recorded by a 3D acoustic Doppler velocimeter (ADV) and stored on data logger software on the attached computer system. The wave breaking point was estimated in preliminary experiments according to studied geometry, and the velocimeter was installed on the coastline to record the wave velocity at the breaking moment. Waves can break by changing in either the entrance slope of the shore or the still water depth (Jalil-Masir et al. 2021). Here, the primary slope and still water depth were determined based on previous studies to ensure breaking of waves with different heights reaching the flat shore.

### Experiment steps

A 8.6-m-long flume was divided longitudinally into three parts: 2 m for the tank, 3 m for the model, and 3.6 m for the downstream. The tank was created first by placing a Plexiglas plate at the beginning of the flume and then by installing a sliding metal gate 2 m from the plate. The gate was opened using a thread-and-spool mechanism made up of a tow rope and weights. The water depth behind the sliding valve was modified for various pipes with the still water level along the shore set at 7 cm. Meeting the objectives of the present study

required the generation of waves broken at the front of the study area. The wave height simulation was performed using a 1:50 scale and the solitary wave theory (Russell, 1845; Ratnasooriya et al. 2008). In the laboratory, behind-the-gate water depths of 25.6, 39.5, and 47 cm from the flume bed could yield wave heights of 6, 9, and 12 cm, respectively, at the front of the coast.

In physical modeling, since the ratio of two forces (surface friction and driving body) increases or decreases, inherent uncertainties are unavoidable, but they can be acceptable in a specific flow condition, if the range of the modeling scale is selected appropriately. Hence for good physical modeling which normally hindered by uncertainties in the selected scale and constraints in the experiments, this research selected the 1:50 scale that lies in the 1:30–1:60 range (accepted for coastal waves modeling; Heller 2011) so that the results are least affected. Considering 10 m as the full-scale height for a tree, which lies in the 8–12 m range and is quite acceptable for a middle age coastal palm tree, this study assumed (based on its selected scale) 0.25 m as the tree height in its modeling. In this research, the wave velocity ranged from 1.30 to 1.5 m/s (full scale: 9–11 m/s, according to the Froude number similarity) and wave height varied in the 0.06–0.12 m range (full scale: 3–6 m). Shafiei et al. (2016) have reported 4–16 m/s and 3–15 m as the ranges of the wave velocity and wave height for a real tsunami, and those of the current study fall within these ranges.

To simulate the coast, a movable plate was placed in the flume and the rigid vegetation was placed on top of it. The load cell was connected to the plate to measure the wave-induced force. For the first time, the maximum wave force absorbed by the coastal forest was measured directly.

Experiment videos recorded by a high-speed camera were converted into images which were then analyzed to calculate the wave height at each point of the coastline. An ADV was used to measure the velocity at the point before the wave began to break. Experiments were carried out with and without TCF. To model the trees, a structure of 32-cm-high and 9 mm-diameter rigid plastic cylinders was used (Akgul et al. 2013; Sundar et al. 2011; Huang et al. 2011).

Placed $5 \times 5$, $10 \times 10$, $15 \times 15$, and $20 \times 20$ cm apart on the coast plate in two parallel (P) and staggered (S) arrangements, the TCF cover was 40 and 45 cm long (normal to the flow direction) and 15, 30, 45, and 60 cm wide (extended in the flow direction). Here $D_v = \frac{Q \times G}{T}$ where $Dv$ is the density number (stems/m$^2$), $Q$ is the number of stems/m$^2$ in each arrangement, $G$ is the number of stems in each experiment (for the width and distance among the trees in each arrangement), and $T$ is the number of stems per unit width along the TCF cover length in each arrangement. Considering the definition of density, the number of cover rows (normal to the flow) and obtained densities were identical in both arrangements. However, the number

of trees and the way they were arranged against the wave were different. Figures 1, 2 and 3 show the experimental setup and TCF arrangements. Table 1 lists the cover placement conditions. In all experiments, the cover increased in the direction of coast.
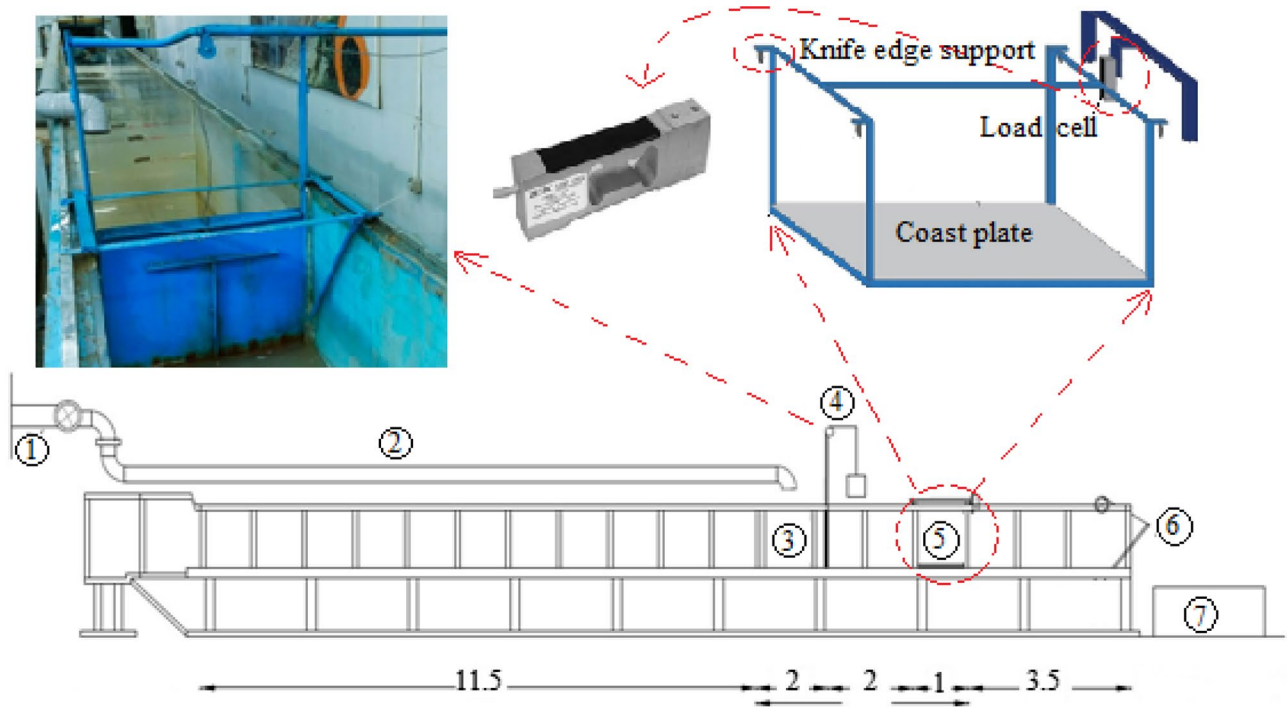


All dimensions are in meters

1- The main water pipe   2- Inlet water pipe to the wave tank 3-Wave head supply tank 4-Sliding gate
5- Movable frame (with knife edge support) 6-End valve 7-Flow drainage tank

**Fig. 1** Side view of the flume with the equipment
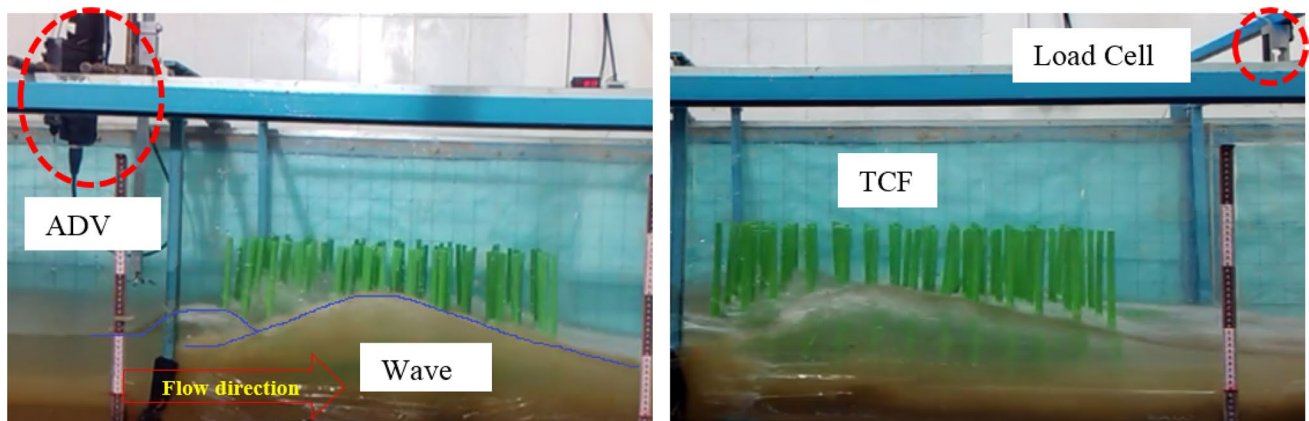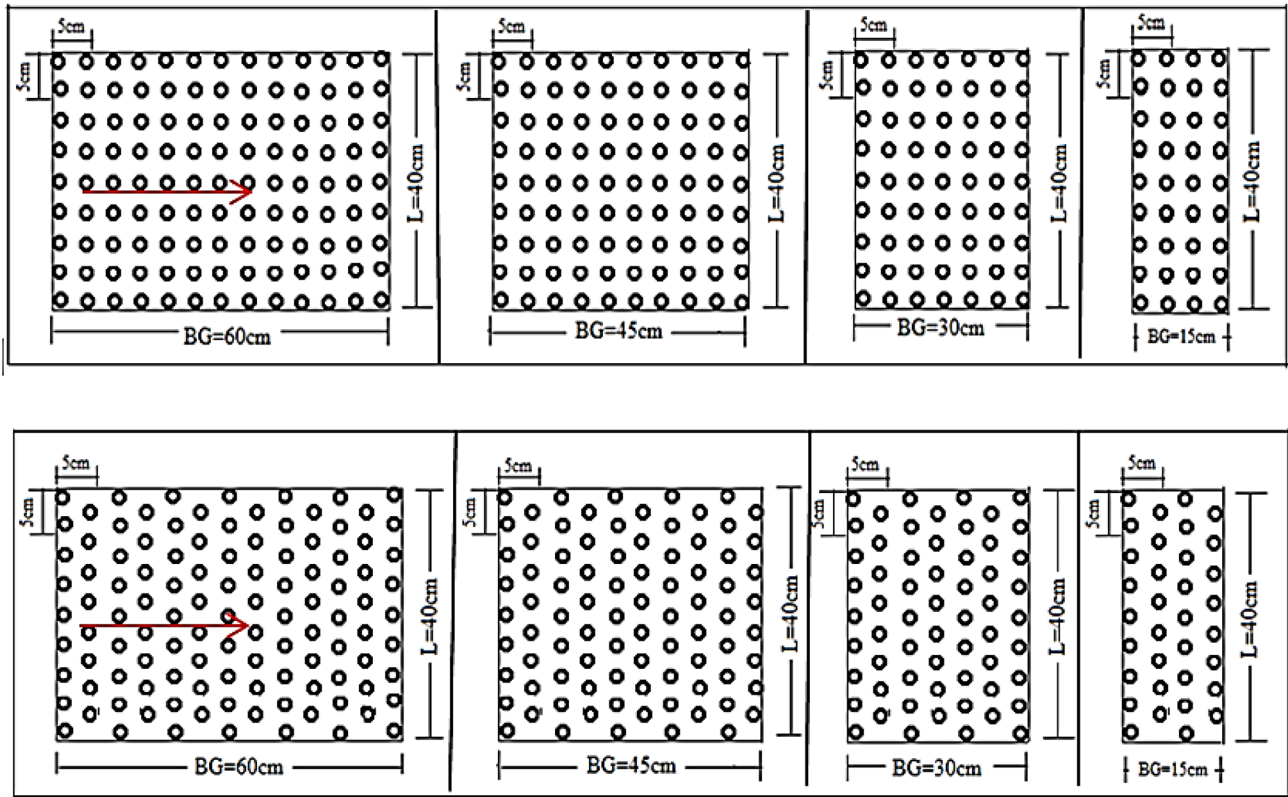


**Fig. 2** Experimental setup

**Fig. 3** TCF in staggered and parallel arrangements in 4 widths and shortest inter-tree distance * Flow direction →

**Table 1** Cover characteristics

| Distance between the trees (cm×cm) | Number of rows | Density number (stems/m$^2$) | Number of tree | | Parallel | Staggered |
|---|---|---|---|---|---|---|
| | | | Parallel | Staggered | | |
| 20×20 | 4 | 24 | 12 | 10 | P1 | S1 |
| | 3 | 18 | 9 | 8 | | |
| | 2 | 12 | 6 | 5 | | |
| 15×15 | 5 | 40 | 20 | 18 | P2 | S2 |
| | 4 | 32 | 16 | 14 | | |
| | 3 | 24* | 12 | 11 | | |
| | 2 | 16 | 8 | 7 | | |
| 10×10 | 7 | 77 | 35 | 31 | P3 | S3 |
| | 6 | 66 | 30 | 27 | | |
| | 4 | 44 | 20 | 18 | | |
| | 3 | 33 | 15 | 14 | | |
| 5×5 | 13 | 273 | 117 | 111 | P4 | S4 |
| | 10 | 210 | 90 | 85 | | |
| | 7 | 147 | 63 | 60 | | |
| | 4 | 84 | 36 | 34 | | |

*Density number for 15×15 configuration to distinguish from that for 20×20 configuration
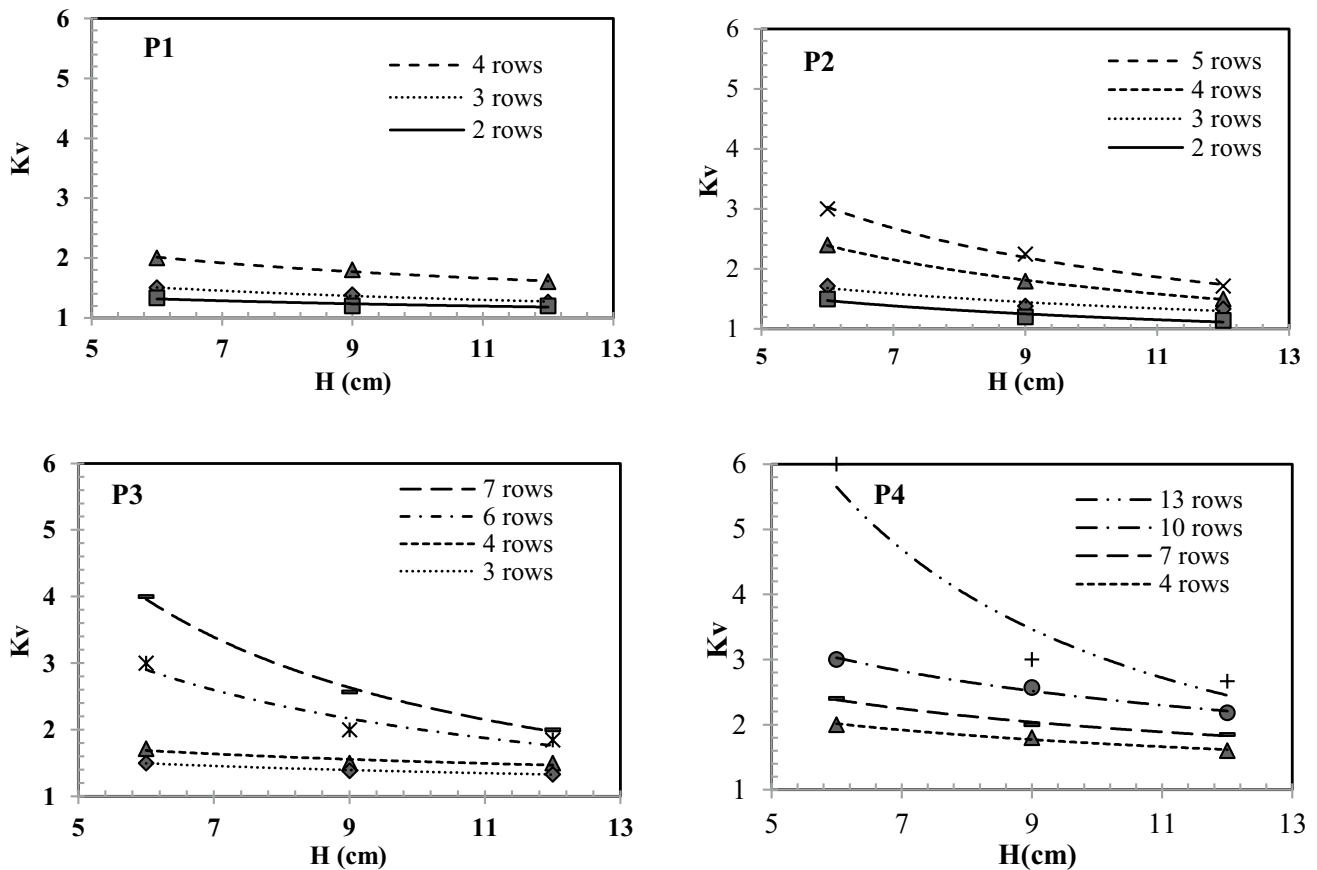
**Fig. 4** $K_v$ ratio for different pre-cover wave heights in parallel arrangement, ($P_1$–$P_4$)

## Results and discussion

### TCF effects on the wave height reduction in the form of damping rate

Figures 4 and 5 show the wave dissipation rate ($\frac{H}{H_0}$) in two arrangements (named P and S). TCF effect on the wave damping was studied by $K_v$.

When a wave hits the coast, it faces a cover-caused drag as a resistive force and loses part of its driving force to resist the drag. Recorded data showed that, in general, the wave height reduction depends on cover features, such as arrangement, inter-tree distance, and cover width.

In fixed tree intervals, increasing the TCF width decreased the post-cover wave height. As wave hits a higher number of trees, the drag resistive force increases and more energy is absorbed by the cover from the wave.

Studies on $K_v$ showed that following an increase in the width and a decrease in the tree distance, the wave damping either increases or, in some cases, remains relatively unchanged. According to the observations, the difference in wave height reduction rate between the highest (13) and

lowest (2) number of the TCF rows was 50% at the highest inflow wave height (12 cm).

Table 2 shows $K_v$ based on the inflow wave height for different parallel-mode TCF densities. Considering the results of the present study and those found by Yin et al. (2017) and Lou et al. (2018), who used the post-cover to pre-cover wave height ratio to determine the damping rate, a rise in the row numbers and a fall in the tree cover distance could decrease the wave height and increase its damping rate. TCF interferes with the wave propagation and leads to increased friction, turbulence, wave breaking, and hence, reduced wave energy. However, at low densities where the coast-TCF resistance against the waves is low, the wave height reduction rate decreases and $K_v$ tends to reach zero. The increase in the TCF density from 12 to 273 (stem/m$^2$) reduced the post-cover wave height by 4.62 times. The staggered mode was more effective than parallel mode in wave damping (by 24% averagely). The rate of wave height reduction in terms of the effect on trees ($K_v^* = 1 - \frac{H_0}{H}$) is presented in Table 2. As shown in Table 2, the TCF effect on the wave energy loss due to reduced wave height was up to 81%. The rate of wave height reduction reported by Ratnasooriya et al. (2008)
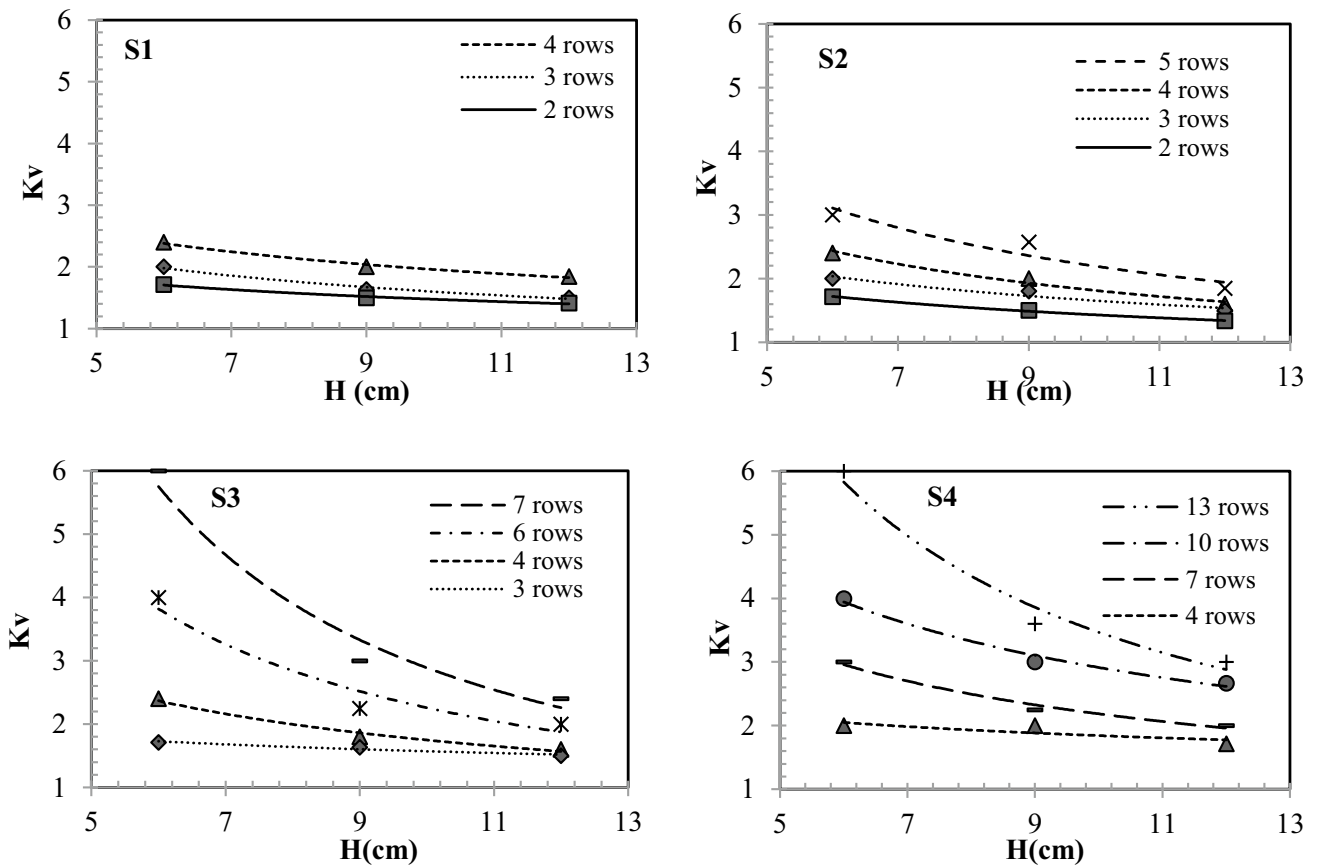
**Fig. 5** $K_v$ ratio for different pre-cover wave heights in staggered arrangement, $(S_1-S_4)$

**Table 2** Damping rate for different TCF densities

| Density | | 24 | 18 | 12 | 40 | 32 | 24* | 16 | 77 | 66 | 44 | 33 | 273 | 210 | 147 | 84 |
|---|---|---|---|---|---|---|---|---|---|---|---|---|---|---|---|---|
| Parallel | $K_v$ | 1.80 | 1.38 | 1.24 | 2.32 | 1.90 | 1.48 | 1.28 | 2.86 | 2.28 | 1.57 | 1.41 | 3.89 | 2.58 | 2.08 | 1.80 |
| | $K_v^*$ | 0.56 | 0.73 | 0.81 | 0.46 | 0.55 | 0.69 | 0.80 | 0.38 | 0.43 | 0.67 | 0.72 | 0.30 | 0.40 | 0.49 | 0.57 |
| Staggered | $K_v$ | 2.08 | | 1.71 | 1.54 | 2.47 | 2.00 | 1.77 | 1.52 | 3.80 | 2.75 | 1.93 | 1.62 | 4.20 | 3.22 | 2.42 |
| | $K_v^*$ | 0.49 | 1.00 | 0.59 | 0.65 | 0.42 | 0.51 | 0.57 | 0.67 | 0.31 | 0.40 | 0.53 | 0.62 | 0.26 | 0.32 | 0.43 |

and Irtem et al. (2009) for coastal vegetation varies in the 40–45% range. Causes of this difference can be such laboratory conditions as the features of coast and coastal forest cover and the wave height or the experiments scale.

## TCF effects on the wave force absorption

TCF effect on wave force reduction was studied as the cover efficiency to generate drag force against the waves. The absorbed forces were recorded by a dynamometer in with-TCF and no-TCF states. Figures 6 and 7 show the results as the Ft diagram in terms of the inflow wave heights in parallel and staggered modes.

Figures 6 and 7 show the effects of rows (TCF width), spacing, and arrangements on reducing the wave force and show that, in general, the absorbed forces increased compared with no-cover case. In the densest case (width of 60 cm and distance of $5 \times 5$ cm), with the staggered arrangement and wave heights of 6, 9 and 12 cm, the force damping rate increased 3.22, 3.4 and 4.7 times, respectively. Four different aspects were studied to evaluate the TCF effects on the wave force:

### Constant wave height and TCF width and variable distance

In general, a reduced distance increased the load cell-recorded force. Based on Table 3, at maximum cover width
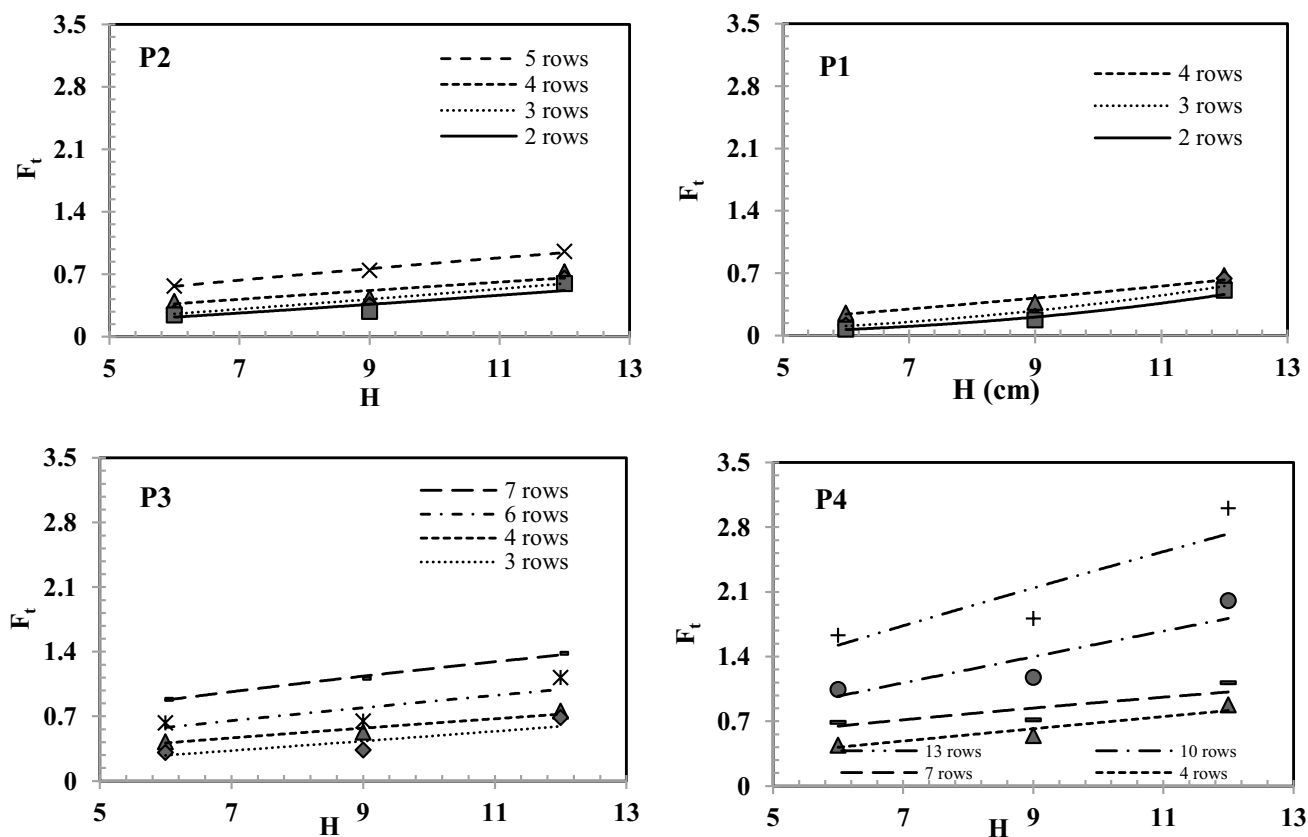
**Fig. 6** Dimensionless force ratio ($F_t$), against wave height for the parallel arrangement, (P1–P4)

and wave height, and in parallel arrangement, the absorbed force increased 0.68, 1.049, and 1.4 times, in the $5 \times 5$ cm distance compared with $10 \times 10$, $15 \times 15$, and $20 \times 20$ cm distances, respectively. In other widths as well, this tendency persisted. In reality, the greater breadth may absorb more force from the waves because to the higher density number and tree resistance. In all instances, the densest cover in the staggered configuration had the best force-absorbing efficacy (3.76 times more than that of the no-cover case).

### Constant tree distance and wave height and variable width

This result shows that at a fixed distance, an increase in width increased the absorbed force because more cover rows against waves can absorb more force. According to Table 4, at the minimum distance ($5 \times 5$ cm) and wave height (6 cm), and in parallel arrangement, the absorbed force increased, in width of 60 cm, 0.287, 0.555 and 0.825 times compared with widths of 45, 30 and 15 cm, respectively. At the maximum $20 \times 20$ cm distance, although the number of rows and hence number of trees increased, the absorbed force did not increase significantly in each width, possibly in terms of the long inter-row and inter-tree distances (in a row). Since trees lie in the flow path and flow is separated over their

bodies, a wake zone is formed behind each tree. When trees are placed in the front tree's wake zone, the latter's effectiveness virtually declines since its real effective absorbing surface is diminished. However, when trees are excessively apart, their group effect is practically reduced and each tree alone, instead of several, stands against the wave causing it to break and not function properly, especially in front rows. It was assumed that the tree does not break or bend against the stream.

In general, maintaining the optimal inter-tree distance has shown to be of great importance and needs additional studies and experiments for correct determination.

### Constant width and tree distance and variable inflow wave height

The results show that an increase in the wave height increased the absorbed force. For instance, in a 60-cm width and a $10 \times 10$ cm distance, absorbed wave force increased by 3.217 and 0.613 times at 12 cm height compared with 6 and 9 cm, respectively. In fact, a height increase causes the wave to hit the cover faster, more drag force to be created from the cover (because of increased contact surface and hitting velocity), and more force to be absorbed from the waves.
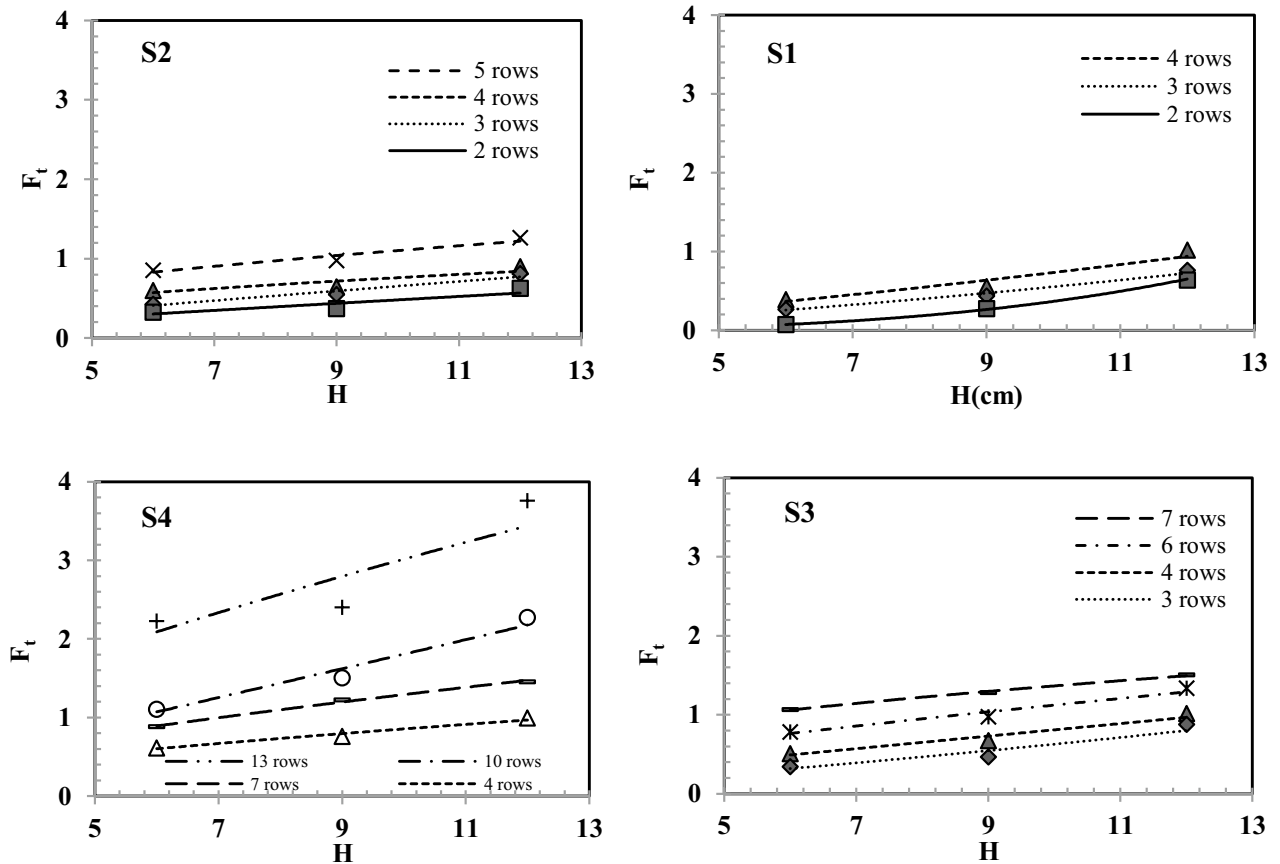
**Fig. 7** Dimensionless force ratio ($F_t$), against wave height for the staggered arrangement, (S1–S4)

**Table 3** Absorbed wave force (N); width, 60 cm; wave height, 12 cm; arrangements, P and S

| Absorbed wave force | | | | |
|---|---|---|---|---|
| Distance (cm×cm) | 5×5 | 10×10 | 15×15 | 20×20 |
| Parallel | 160.29 | 95.31 | 78.2 | 66.96 |
| Staggered | 190.29 | 100.26 | 90.58 | 80.74 |
| No TCF | 40 | | | |

**Table 4** Absorbed wave force (N); cover distance, 5×5(cm×cm); wave height, 6 cm; arrangements, P and S

| TCF Width (cm) | | 15 | 30 | 45 | 60 |
|---|---|---|---|---|---|
| F(N) | Parallel | 17.3 | 31.58 | 24.52 | 31.58 |
| | Staggered | 19.36 | 38.71 | 25.27 | 38.71 |
| | No TCF | 12 | | | |

## Arrangement effects

Results (Tables 3 and 4) show that the staggered arrangement was more effective in all comparisons than the parallel arrangement reduce the waves force.

The maximum difference in absorbed force between two arrangements was reported to be 29.5% in the density of 147.

## TCF effects on the drag coefficient

To study the effects of TCF on drag coefficient, the drag coefficient variations was plotted against the forces absorbed from waves for each parallel (Fig. 8) and staggered mode (Fig. 9).

As seen in Figs. 8 and 9, an increase in rows and cover widths and a decrease in inter-cover distances increased drag coefficient and the force. For instance, at a wave height of 9 cm and a fixed distance of 5×5 cm, increasing rows from 4 to 13 increased the drag coefficient by 36.65%. At the same wave height, a fixed cover width (60 cm), and a variable distance, reducing the distance from 20×20 cm to 5×5 cm, for example, increased the drag coefficient by 27.54%, because more wave force was absorbed and dissipated by the cover due to more number of rows against the wave and more applied resistance. The staggered arrangement was more effective than the parallel arrangement in absorbing the wave force and consequently increasing the
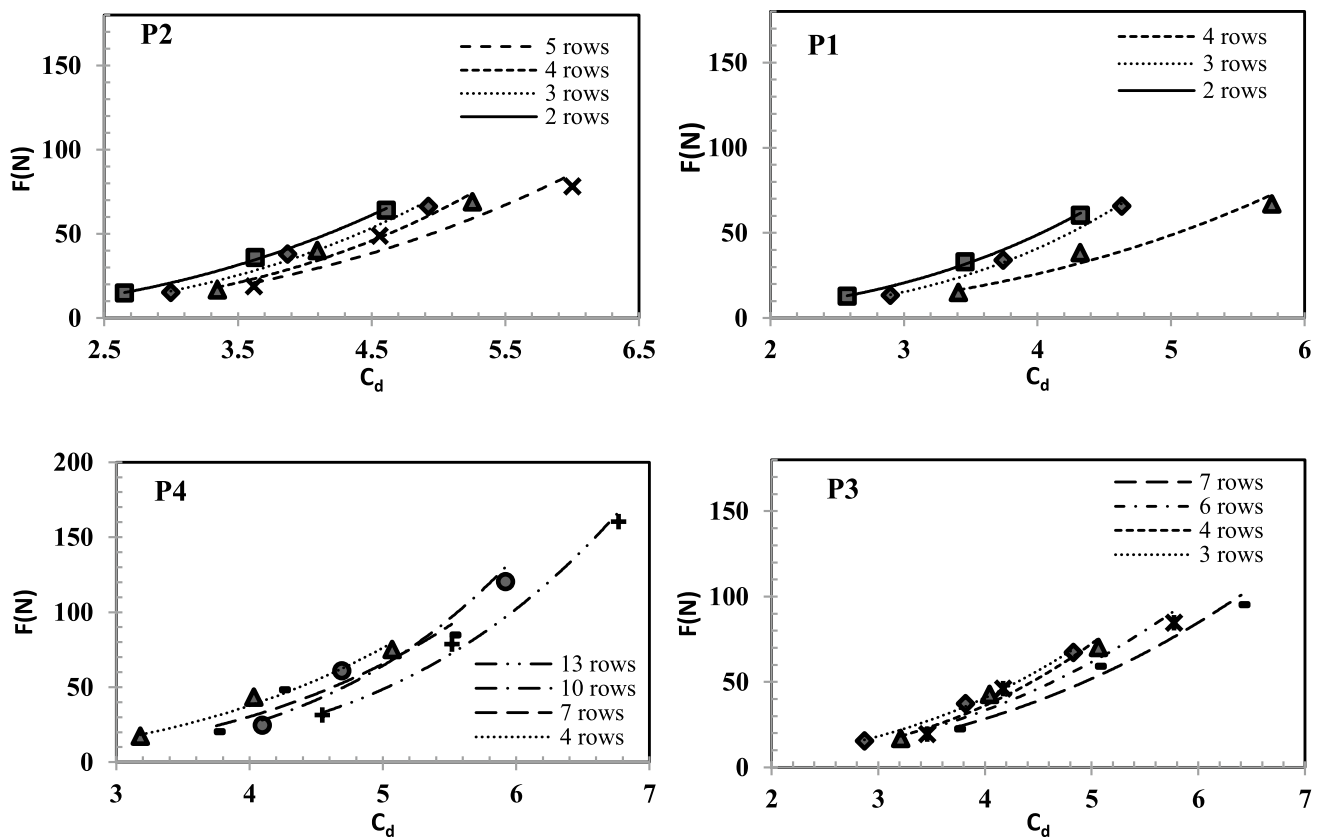
**Fig. 8** Drag coefficient versus force for parallel arrangement, (P1–P4)

drag coefficient. The impact surface against the wave in the staggered state is greater than it is in the parallel state due to the different arrangements of the cover. Hence, when the wave hits the staggered cover, the drag force resistance against the wave passage is higher. As inter-tree distance decreases, the graphs become denser because force variations with the drag coefficient are more scattered at longer distances, to some extent showing TCF inter-tree distance and density effects, as major factors, on the force absorbed from the waves.

## TCF width effects on the drag coefficient

Figures 10 and 11 show that reduced cover rows reduced the drag coefficient; the addition of one cover row increased the drag coefficient by averagely 9.7%. Increasing the width and rows increases the cover resistance against the flow, and hence, more force is drawn from the wave causing the drag coefficient to increase. However, drag coefficient increase rate was not a fixed or an absolute increase because after a certain value, known here as the optimal limit, the growth intensity was reduced. In other words, after the optimal

limit, the drag coefficient increase rate did not justify the row increase in regard to economic/administrative issues (although no accurate economic calculations were done).

Drag coefficient increase was addressed in maximum and minimum distances, and the optimal limit was obtained at the highest wave height (12 cm) and for each inter-tree distance. For instance, at a $20 \times 20$ cm distance in both arrangements, a row increase from 2 to 3 and from 3 to 4 added 7.94 and 16.38% to the drag coefficient, respectively. In fact, a row increase from 2 to 4 caused the drag coefficient to reach from 4.72 to 5.93, which means in the 4-row case, the share of the first 2 rows was 79% and that of the next 2 rows was only 21%.

At a $5 \times 5$ cm distance, increasing the rows from 4 to 7, 7 to 10, and 10 to 13 increased the drag coefficient by 8.43, 8.02, and 11.89%, respectively. In fact, an increase of 9 rows raised the drag coefficient by 30%, while the first 4 rows increased the drag coefficient by around 70%, causing the rise from 4 to 13 to cause the drag coefficient to reach from 5.41 to 7.06 (in a 13-row arrangement). In $5 \times 5$ cm inter-tree distance, the drag coefficient intensity reduced for each cover row increase. In $20 \times 20$ cm distance, the drag coefficient
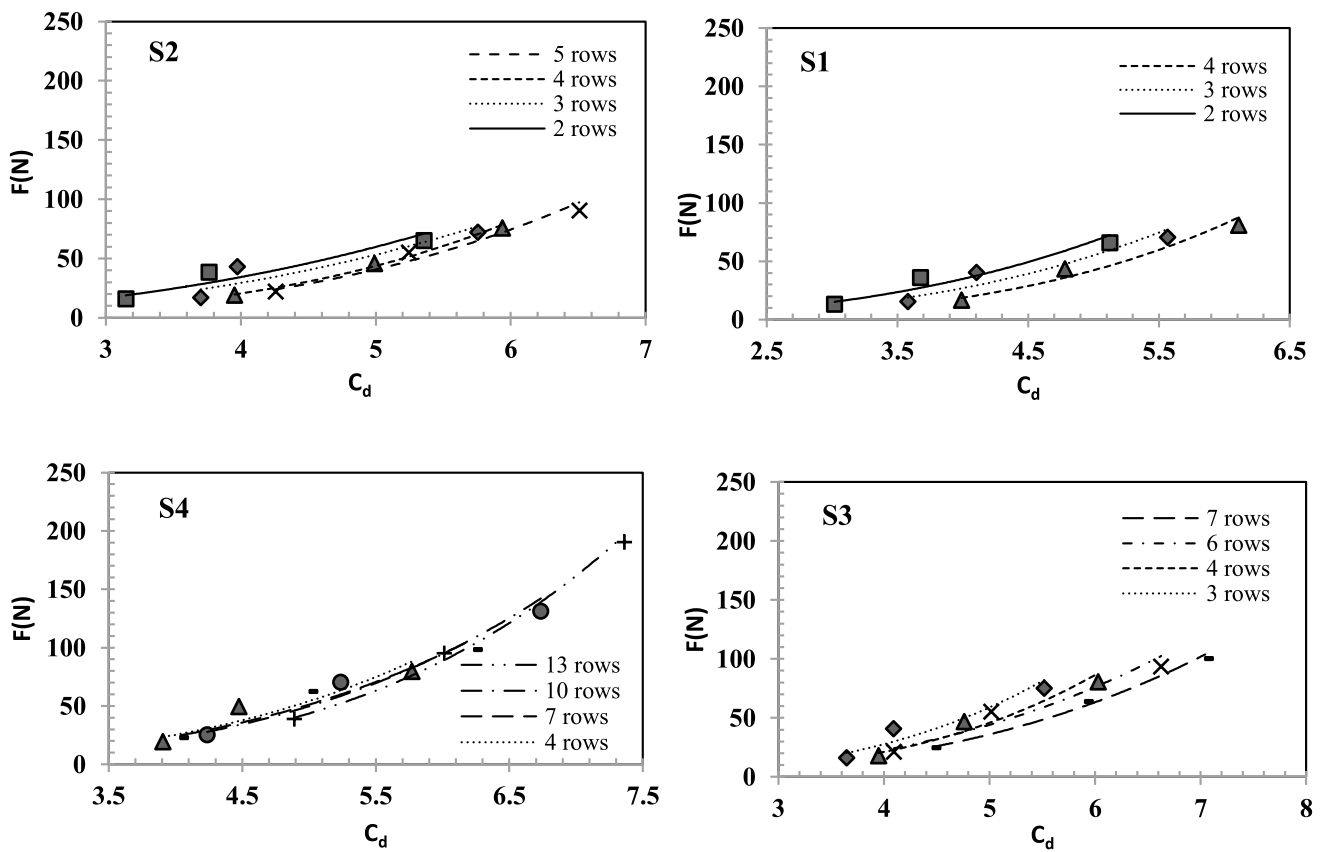
**Fig. 9** Drag coefficient against force for staggered arrangement, (S1–S4)

increase rate for each cover row was higher indicating a better cover performance. As mentioned earlier (Sect. 3–2-2), further studies need to be conducted on determining the optimum distance value and to use the wake zone created by each tree as a basis to place the next one.

### TCF density effects on the drag coefficient

As shown in Fig. 12, an increase in the density and in the number of rows increased both the drag coefficient and cover resistance against the flow. Increasing the density increased drag coefficient and cover resistance by 62.32 and 54.31%, in staggered and parallel arrangement respectively. Comparing two arrangements (Fig. 12) reveals that the staggered mode was more efficient than the parallel mode (averagely 11.38%) in showing more resistance against the wave.

Although an increase in the drag force with the TCF density is mainly due to an increase in the area that absorbs the force, scale, wave height and TCF (type, material, density and definition) too affect the drag coefficient considerably. Previous studies have estimated lower values for the drag coefficient because they have defined the force-absorbing area differently and estimated higher force values, which

can be attributed to their using of different tree simulation models that, instead of cylinders, used trees with branches and foliage. For instance, Hirashi and Harada (2003) and Huang et al. (2011) have reported drag coefficients in the 1–1.5 range and 1.5–2 range, respectively.

### A relationship for estimating the drag coefficient ($C_d$)

Statistical analyses were used to study the interaction effects of extracted dimensionless parameters on the drag coefficient and to present a mathematical relationship (Eq. 10) to predict the related values as follows:

$$C_d = 8.882\left(H/h_v\right)^{0.702} + 0.152\left(\frac{\tau_v}{\rho_w V^2}\right)^{0.1},  \tag{10}$$

where $C_d$ is the drag coefficient, $\frac{H}{h_v}$ is the relative immersion (dimensionless ratio of the wave incident height to the tree height) and dimensionless $\frac{\tau_v}{\rho_w V^2}$. Equation (10) is extracted using 70% of the data recorded from the experiments and then validated using the remaining 30%. The selection of
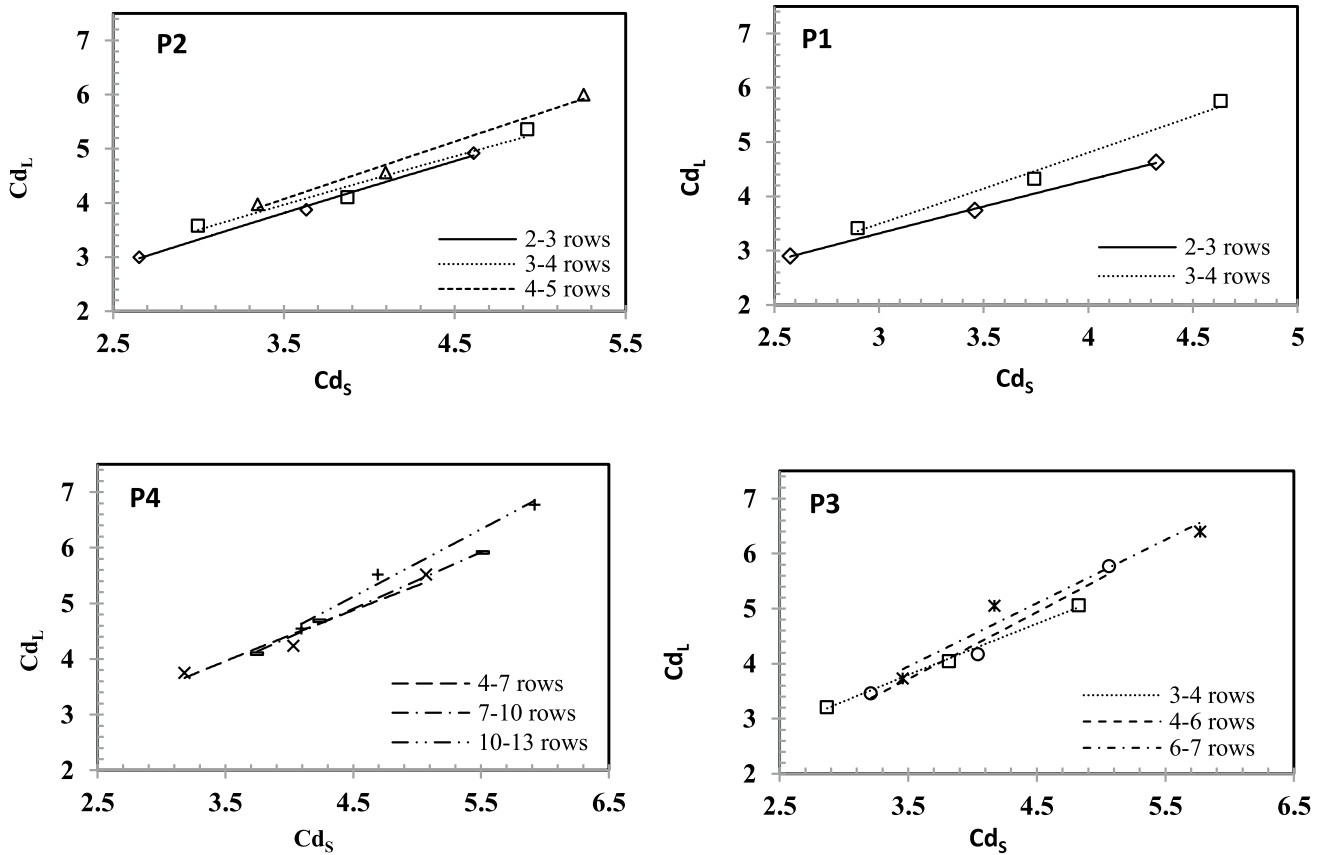
**Fig. 10** Effects of the cover row increase on the drag coefficient in parallel mode, (P1–P4) *Drag coefficient of smaller tree group: $Cd_S$, Drag coefficient of longer tree group: $Cd_L$

these parameters is based on the sensitivity analysis performed for all independent parameters with the dependent parameters.

As seen in the statistics evaluations (Table 5), the results that calculated via Eq. (10) were acceptably accurate and the predicted value of the drag coefficient was close to experimental results. The correlation coefficient (R square) and efficiency coefficient (CE) of this formula were close to 1 (representing a perfect correlation and a good model), since the NRMSE range is $(0, +\infty)$, and it was near zero here, and the simulation is excellent accurate ($< 10\%$) (Jamieson et al. 1991). Also since $P$ value $< 0.05$, the proposed formula is acceptable at 95% confidence level. As shown in Fig. 13, the correlation is relatively high because the points are closely scattered around the 45° line.

When laboratories have limitations, relations found in this research can be used in similar cases with the same accuracy. However, this study has used dimensionless ratios effective on the studied phenomenon to maintain the all-inclusiveness of the presented formula; hence, it can be generalized to reality as well. But, using the results under different conditions needs future experiments.

In addition to using statistical and mathematical methods to define a model for predicting the studied parameter, data-based methods can also be used. Machine learning models have been recently used in certain researches on the costal phenomena; hence, we suggest they be used in future studies, too, to find appropriate formula (Ghanbari-Adivi et al. 2022; and Jalil-Masir et al. 2022).

## Conclusion

This research addressed the effective contributions of TCF to protection against the long waves in tsunami/storm conditions. By direct measuring of trees drag forces and waves velocities, TCF efficiency to create the resistive forces and in wave force absorption/attenuation was investigated in the form of drag force.

The effects of cover density, distance, width, arrangement, and wave height on wave force absorption were also looked at in order to attain a better drag coefficient. Particularly at higher densities and wider cover widths, more variances were observed. The drag coefficient grew as the
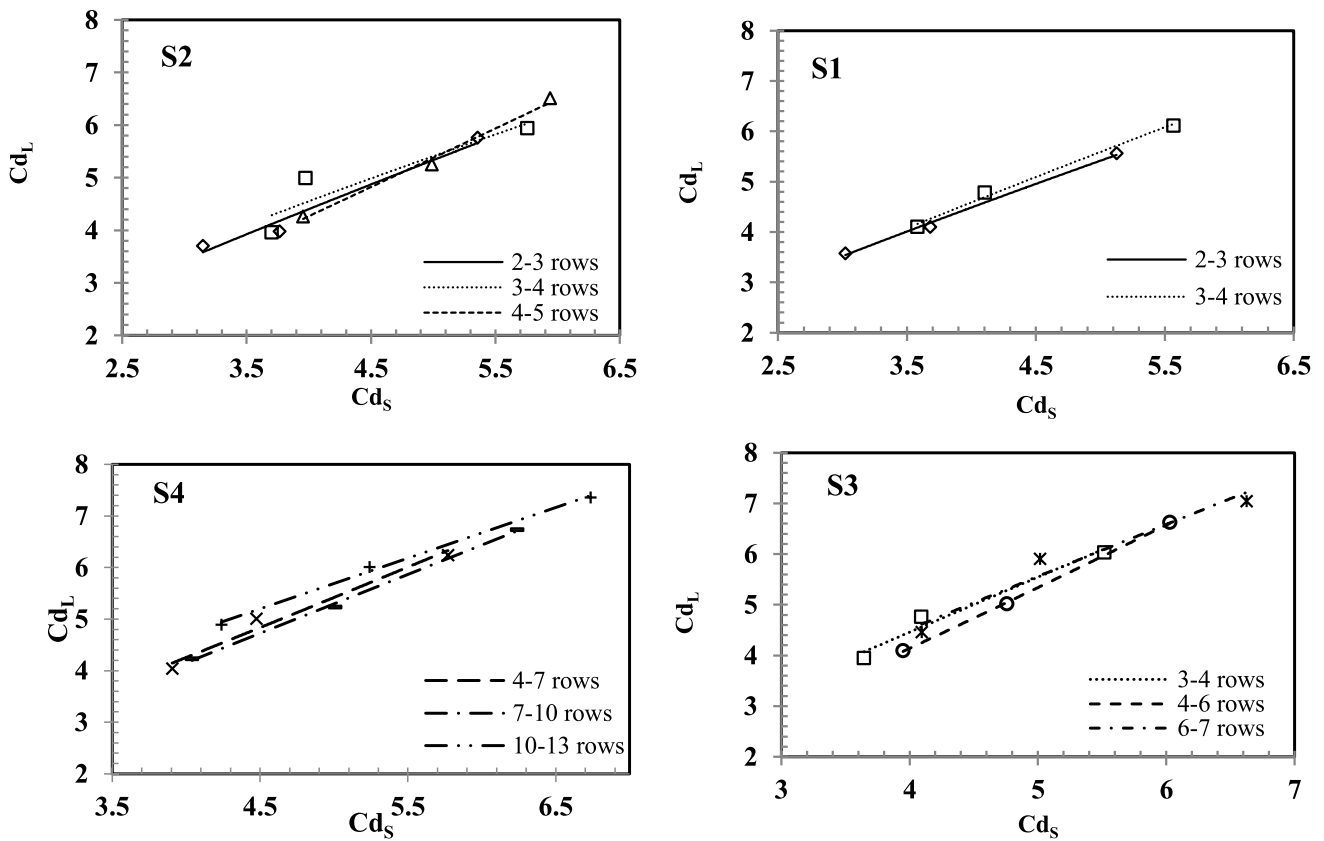
**Fig. 11** Effects of cover row increase on the drag coefficient instaggered mode, (S1–S4)
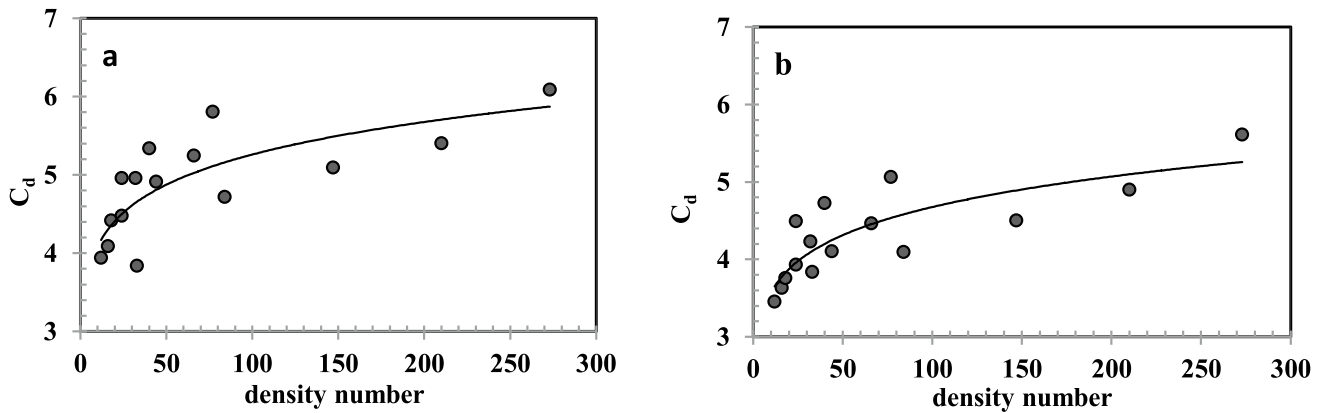


**Fig. 12** Drag coefficient against the TCF density (a: Staggered, b: Parallel)

**Table 5** Evaluation statistics of the drag coefficient estimation formula

| R square | NRMSE | P value | CE |
|----------|-------|---------|-----|
| 0.97 | 0.09 | < 0.05 | 0.89 |

number of rows, cover widths, and inter-tree spacing all increased. So that increasing the width of the covered area by 4 times increases the drag coefficient by about 26%, and reducing the inter-tree distance by 75% increases it by about 20%, but it has not highly increased with a decrease in the
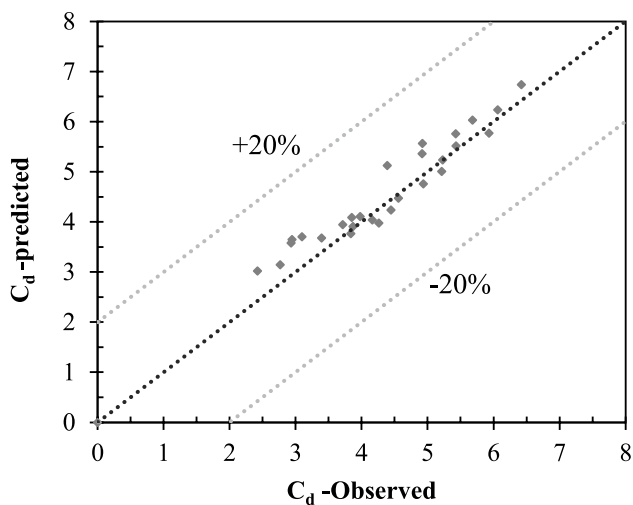
**Fig. 13** Comparison of the observed drag coefficient with the predicted one by Eq. (10)

distance or an increase in the width. Under the smallest/largest inter-tree distances, an increase in the cover rows reduces/increases the drag coefficient. In fact, the inter-tree distance and drag coefficient are inversely related, i.e., for a specified number of trees, a $20 \times 20$ tree arrangement performs better than other arrangements with smaller inter-tree distances (same No. of trees); among the cases examined in this research, this superiority is estimated to be, averagely, 24%. As reducing the inter-tree distance naturally increases the resistance, but imposes more implementation costs, determining an optimal density including optimal inter-tree distance and optimal width for the cover area is a very important initial step in implementing such plans.

On the other hand, at a given cover width, the effects of the back rows on the total drag were less than those of the front rows. The intensity of increased drag coefficient in a known width with more trees is a highly important factor on enhancing the coastal cover performance against the waves.

Increasing the number of rows of trees from 2 to 4 rows had increased the drag coefficient by about 29%, but increasing the number of rows of trees from 4 to 13 rows only increased the drag coefficient by 33%. Further studies need to be conducted on determining the optimum distance. Since the post-cover wave height reduction has not been significant in small widths and large inter-tree spacing, determining the optimum distance is important to prevent group effect being reduced to a single-tree effect.

Studies showed that the staggered arrangement was shown to be more efficient than the parallel layout. Staggered tree arrangement, compared with the parallel form, has increased the drag coefficient by about 14.5%, averagely.

Explaining the effects of coastal conditions on wave-caused drag force, practically with independent measurable wave-coast variables, enables a better understanding and estimation of drag coefficient to evaluate numerical models. Finally, a relationship with acceptable accuracy was presented to predict the drag coefficient with a correlation coefficient of 0.97.

## Declarations

**Conflict of interest** The authors declare that they have no known competing financial interests or personal relationships that could have appeared to influence the work reported in this paper.

## References

Akgul MA, Yilmazer D, Oguz E, Kabdasli MS, Yagci O (2013) The effect of an emergent vegetation (ie Phragmistes Australis) on wave attenuation and wave kinematics. J Coast Res 65:147–152. https://doi.org/10.2112/SI65-026.1

Augustin LN, Irish JL, Lynett P (2009) Laboratory and numerical studies of wave damping by emergent and near-emergent wetland vegetation. Coast Eng 56(3):332–340. https://doi.org/10.1016/j.coastaleng.2008.09.004

Baptist M.J. (2005) Modelling floodplain biogeomorphology. Delft University of Technology, Faculty of Civil Engineering and Geosciences, Section Hydraulic Engineering, Delft, pp 213

Bradley K, Houser C (2009) Relative velocity of seagrass blades: implications for wave attenuation in low-energy environments. J Geophys Res. https://doi.org/10.1029/2007JF000951

Buckingham E (1914) On physically similar systems; illustrations of the use of dimensional equations. Phys Rev 4(4):345–376. https://doi.org/10.1103/PhysRev.4.345

Cao H, Feng W, Hu Z, Suzuki T, Stive MJ (2015) Numerical modeling of vegetation-induced dissipation using an extended mild-slope equation. Ocean Eng 110:258–269. https://doi.org/10.1016/j.oceaneng.2015.09.057

Cavallaro L, Re CL, Paratore G, Viviano A, Foti E (2011) Response of Posidonia oceanica to wave motion in shallow-waters-preliminary experimental results. Coast Eng Proc 32:49–49

Chen M, Lou S, Liu S, Ma G, Liu H, Zhong G, Zhang H (2020) Velocity and turbulence affected by submerged rigid vegetation under waves, currents and combined wave–current flows. Coast Eng 159:103727. https://doi.org/10.1016/j.coastaleng.2020.103727

Dalrymple RA, Kirby JT, Hwang PA (1984) Wave diffraction due to areas of energy dissipation. J Waterw Port Coast Ocean Eng 110(1):67–79. https://doi.org/10.1061/(ASCE)0733-950X(1984)110:1(67)

Dias JA (2004) A história da evolução do litoral português nos últimos vinte milénios. *Tavares, AA, Tavares, MJF & Cardoso, JL, Evolução Geohistórica do Litoral Português e Fenómenos Correlativos: Geologia, História, Arqueologia e Climatologia*, pp. 157–170

Esteban M, Roubos JJ, Iimura K, Salet JT, Hofland B, Bricker J, Ishii H, Hamano G, Takabatake T, Shibayama T (2020) Effect of bed roughness on tsunami bore propagation and overtopping. Coast Eng 157:103539. https://doi.org/10.1016/j.coastaleng.2019.103539

Fathi-Moghadam M, Davoudi L, Motamedi-Nezhad A (2018) Modeling of solitary breaking wave force absorption by coastal trees.

Ocean Eng 169:87–98. https://doi.org/10.1016/j.oceaneng.2018.09.021

Foster NM, Hudson MD, Bray S, Nicholls RJ (2013) Intertidal mudflat and saltmarsh conservation and sustainable use in the UK: a review. J Environ Manage 126:96–104. https://doi.org/10.1016/j.jenvman.2013.04.015

Gaertner-Mazouni N, De Wit R (2012) Exploring new issues for coastal lagoons monitoring and management. Estuar Coast Shelf Sci 114:1–6. https://doi.org/10.1016/j.ecss.2012.07.008

Ghanbari-Adivi E, Ehteram M, Farrokhi A, Sheikh Khozani Z (2022) Combining radial basis function neural network models and inclusive multiple models for predicting suspended sediment loads. Water Resour Manage 36(11):4313–4342

Gonçalves SC, Anastácio PM, Marques JC (2013) Talitrid and Tylid crustaceans bioecology as a tool to monitor and assess sandy beaches' ecological quality condition. Ecol Ind 29:549–557. https://doi.org/10.1016/j.ecolind.2013.01.035

Grilli AR, Westcott G, Grilli ST, Spaulding ML, Shi F, Kirby JT (2020) Assessing coastal hazard from extreme storms with a phase resolving wave model: case study of Narragansett, RI, USA. Coast Eng 160:103735. https://doi.org/10.1016/j.coastaleng.2020.103735

Heller V (2011) Scale effects in physical hydraulic engineering models. J Hydraul Res 49(3):293–306. https://doi.org/10.1080/00221686.2011.578914

Hiraishi T, Harada K (2003) Greenbelt tsunami prevention in South Pacific region. Report Port Airport Res Inst 42:1–23

Hsiao SC, Lin TC (2010) Tsunami-like solitary waves impinging and overtopping an impermeable seawall: experiment and RANS modeling. Coast Eng 57(1):1–18

Huang Z, Yao Y, Sim SY, Yao Y (2011) Interaction of solitary waves with emergent, rigid vegetation. Ocean Eng 38(10):1080–1088. https://doi.org/10.1016/j.oceaneng.2011.03.003

Husrin S, Strusińska A, Oumeraci H (2012) Experimental study on tsunami attenuation by mangrove forest. Earth, Planets Space 64(10):973–989. https://doi.org/10.5047/eps.2011.11.008

Irtem E, Gedik N, Kabdasli MS, Yasa NE (2009) Coastal forest effects on tsunami run-up heights. Ocean Eng 36(3–4):313–320

Jalil-Masir H, Fattahi R, Ghanbari-Adivi E, Asadi-Aghbolaghi M (2021) Effects of different forest cover configurations on reducing the solitary wave-induced total sediment transport in coastal areas: an experimental study. J ElsevierOcean Eng 235(1):109350. https://doi.org/10.1016/j.oceaneng.2021.109350

Jalil-Masir H, Fattahi R, Ghanbari-Adivi E et al (2022) An inclusive multiple model for predicting total sediment transport rate in the presence of coastal vegetation cover based on optimized kernel extreme learning models. Environ Sci Pollut Res. https://doi.org/10.1007/s11356-022-20472-y

Jamieson PD, Porter JR, Wilson DR (1991) A test of the computer simulation model ARC-WHEAT1 on wheat crops grown in New Zealand. Field Crop Res 27:337–350

Knutson PL, Brochu RA, Seelig WN, Inskeep M (1982) Wave damping in Spartina alterniflora marshes. Wetlands 2(1):87–104. https://doi.org/10.1007/BF03160548

Leewis L, van Bodegom PM, Rozema J, Janssen GM (2012) Does beach nourishment have long-term effects on intertidal macroinvertebrate species abundance? Estuar Coast Shelf Sci 113:172–181. https://doi.org/10.1016/j.ecss.2012.07.021

Leonardi N, Carnacina I, Donatelli C, Ganju NK, Plater AJ, Schuerch M, Temmerman S (2018) Dynamic interactions between coastal storms and salt marshes: a review. Geomorphology 301:92–107. https://doi.org/10.1016/j.geomorph.2017.11.001

Lima SF, Neves CF, Rosauro NML (2007) Damping of gravity waves by fields of flexible vegetation. Coast Eng 2006(5):491–503. https://doi.org/10.1142/9789812709554_0043

Lou S, Chen M, Ma G, Liu S, Zhong G (2018) Laboratory study of the effect of vertically varying vegetation density on waves, currents and wave-current interactions. Appl Ocean Res 79:74–87. https://doi.org/10.1016/j.apor.2018.07.012

Lövstedt CB, Larson M (2010) Wave damping in reed: Field measurements and mathematical modeling. J Hydraul Eng 136(4):222–233. https://doi.org/10.1061/(ASCE)HY.1943-7900.0000167

Martins MC, Neto CS, Costa JC (2013) The meaning of mainland Portugal beaches and dunes' psammophilic plant communities: a contribution to tourism management and nature conservation. J Coast Conserv 17(3):279–299. https://doi.org/10.1007/s11852-013-0232-9

Mascarenhas A, Jayakumar S (2008) An environmental perspective of the post-tsunami scenario along the coast of Tamil Nadu, India: Role of sand dunes and forests. J Environ Manage 89(1):24–34. https://doi.org/10.1016/j.jenvman.2007.01.053

Maza M, Lara JL, Losada IJ (2015) Tsunami wave interaction with mangrove forests: a 3-D numerical approach. Coast Eng 98:33–54. https://doi.org/10.1016/j.coastaleng.2015.01.002

Mazda Y, Magi M, Ikeda Y, Kurokawa T, Asano T (2006) Wave reduction in a mangrove forest dominated by Sonneratia sp. Wetlands Ecol Manage 14(4):365–378. https://doi.org/10.1007/s11273-005-5388-0

Mendez FJ, Losada IJ (2004) An empirical model to estimate the propagation of random breaking and nonbreaking waves over vegetation fields. Coast Eng 51(2):103–118. https://doi.org/10.1016/j.coastaleng.2003.11.003

Möller I, Spencer T (2002) Wave dissipation over macro-tidal saltmarshes: effects of marsh edge typology and vegetation change. J Coast Res 36:506–521. https://doi.org/10.2112/1551-5036-36.sp1.506

Möller I, Spencer T, French JR, Leggett DJ, Dixon M (1999) Wave transformation over salt marshes: a field and numerical modelling study from North Norfolk, England. Estuar Coast Shelf Sci 49(3):411–426. https://doi.org/10.1006/ecss.1999.0509

Möller I, Kudella M, Rupprecht F, Spencer T, Paul M, Van Wesenbeeck BK, Wolters G, Jensen K, Bouma TJ, Miranda-Lange M, Schimmels S (2014) Wave attenuation over coastal salt marshes under storm surge conditions. Nature Geosci 7(10):727–731

Morison JR, Johnson JW, Schaaf SA (1950) The force exerted by surface waves on piles. J Petrol Technol 2(05):149–154. https://doi.org/10.2118/950149-G

Morris RL, Konlechner TM, Ghisalberti M, Swearer SE (2018) From grey to green: efficacy of eco-engineering solutions for nature-based coastal defence. Glob Change Biol 24(5):1827–1842

Mu H, Yu X, Fu S, Yu B, Liu Y, Zhang G (2019) Effect of stem basal cover on the sediment transport capacity of overland flows. Geoderma 337:384–393. https://doi.org/10.1016/j.geoderma.2018.09.055

Nanko K, Suzuki S, Noguchi H, Ishida Y, Levia DF, Ogura A, Hagino H, Matsumoto H, Takimoto H, Sakamoto T (2019) Mechanical properties of Japanese black pine (Pinus thunbergii Parl.) planted on coastal sand dunes: resistance to uprooting and stem breakage by tsunamis. Wood Sci Technol 53(2):469–489. https://doi.org/10.1007/s00226-019-01078-z

Nardin W, Edmonds DA, Fagherazzi S (2016) Influence of vegetation on spatial patterns of sediment deposition in deltaic islands during flood. Adv Water Resour 93:236–248. https://doi.org/10.1016/j.advwatres.2016.01.001

Nguyen TP, Parnell KE (2017) Gradual expansion of mangrove areas as an ecological solution for stabilizing a severely eroded mangrove dominated muddy coast. Ecol Eng 107:239–243. https://doi.org/10.1016/j.ecoleng.2017.07.038

Nobre AM, Ferreira JG (2009) Integration of ecosystem-based tools to support coastal zone management. J Coast Res 5:1676–1680

Nordstrom KF (2014) Living with shore protection structures: a review. Estuar Coast Shelf Sci 150:11–23. https://doi.org/10.1016/j.ecss.2013.11.003

Quartel S, Kroon A, Augustinus PGEF, Van Santen P, Tri NH (2007) Wave attenuation in coastal mangroves in the Red River Delta Vietnam. J Asian Earth Sci 29(4):576–584. https://doi.org/10.1016/j.jseaes.2006.05.008

Rajendra IA, Sumariati DAR (2018) The role of coconut plants in relation to disaster management in the tropical coastal regions. MATEC Web Conf 229:01012. https://doi.org/10.1051/matecconf/201822901012

Ratnasooriya AHR, Samarawickrama SP, Hettiarachchi SSL, Bandara RPSS, Tanaka N (2008) Mitigation of tsunami inundation by coastal vegetation. J Inst Eng pp 13–19 Sri Lanka. http://dl.lib.mrt.ac.lk/handle/123/11919

Shafiei S, Melville BW, Shamseldin AY (2016) Experimental investigation of tsunami bore impact force and pressure on a square prism. Coast Eng 110:1–16

Sinitsyn AO, Guegan E, Shabanova N, Kokin O, Ogorodov S (2020) Fifty four years of coastal erosion and hydrometeorological parameters in the Varandey region Barents Sea. Coast Eng 157:103610. https://doi.org/10.1016/j.coastaleng.2019.103610

Sorensen RM (2006) Coastal water level fluctuations. Basic Coast Eng. https://doi.org/10.1007/0-387-23333-4_5

Sundar V, Murali K, Noarayanan L (2011) Effect of vegetation on run-up and wall pressures due to cnoidal waves. J Hydraul Res 49(4):562–567. https://doi.org/10.1080/00221686.2010.542615

Suzuki T, Hu Z, Kumada K, Phan LK, Zijlema M (2019) Non-hydrostatic modeling of drag, inertia and porous effects in wave propagation over dense vegetation fields. Coast Eng 149:49–64. https://doi.org/10.1016/j.coastaleng.2019.03.011

Temmerman S, Meire P, Bouma TJ, Herman PM, Ysebaert T, De Vriend HJ (2013) Ecosystem-based coastal defence in the face of global change. Nature 504(7478):79–83. https://doi.org/10.1038/nature12859

Toloui M, Abraham A, Hong J (2019) Experimental investigation of turbulent flow over surfaces of rigid and flexible roughness. Exp Thermal Fluid Sci 101:263–275. https://doi.org/10.1016/j.expthermflusci.2018.10.026

Torita H, Igarashi Y, Tanaka N (2022) Effective management of Japanese black pine (Pinus thunbergii Parlat.) coastal forests considering tsunami mitigation. J Environ Manag 311:114754. https://doi.org/10.1016/j.jenvman.2022.114754

Tschirky P, Hall K, Turcke D (2001) Wave attenuation by emergent wetland vegetation. Coast Eng 2000:865–877. https://doi.org/10.1061/40549(276)67

Türker U, Yagci O, Kabdaşlı MS (2006) Analysis of coastal damage of a beach profile under the protection of emergent vegetation. Ocean Eng 33(5–6):810–828. https://doi.org/10.1016/j.oceaneng.2005.04.019

Van Veelen TJ, Fairchild TP, Reeve DE, Karunarathna H (2020) Experimental study on vegetation flexibility as control parameter for wave damping and velocity structure. Coast Eng 157:103648. https://doi.org/10.1016/j.coastaleng.2020.103648

Wamsley TV, Cialone MA, Smith JM, Ebersole BA, Grzegorzewski AS (2009) Influence of landscape restoration and degradation on storm surge and waves in southern Louisiana. Nat Hazards 51(1):207–224. https://doi.org/10.1007/s11069-009-9378-z

Wang Y, Yin Z, Liu Y (2019) Numerical study of solitary wave interaction with a vegetated platform. Ocean Eng 192:106561. https://doi.org/10.1016/j.oceaneng.2019.106561

Winterwerp JC, Albers T, Anthony EJ, Friess DA, Mancheño AG, Moseley K, Muhari A, Naipal S, Noordermeer J, Oost A, Saengsupavanich C (2020) Managing erosion of mangrove-mud coasts with permeable dams–lessons learned. Ecol Eng 158:106078. https://doi.org/10.1016/j.ecoleng.2020.106078

Yin Z, Yang X, Xu Y, Ding M, Lu H (2017) Experimental wave attenuation study over flexible plants on a submerged slope. J Ocean Univ China 16(6):1009–1017. https://doi.org/10.1007/s11802-017-3298-4

Zhang M, Hao Z, Zhang Y, Wu W (2013) Numerical simulation of solitary and random wave propagation through vegetation based on VOF method. Acta Oceanol Sin 32(7):38–46. https://doi.org/10.1007/s13131-013-0330-4

Zinke P, Olsen NRB, Bogen J (2011) Three-dimensional numerical modelling of levee depositions in a Scandinavian freshwater delta. Geomorphology 129(3–4):320–333. https://doi.org/10.1016/j.geomorph.2011.02.027